Chemosphere xxx (xxxx) xxx

Contents lists available at ScienceDirect

Chemosphere

journal homepage: www.elsevier.com/locate/chemosphere

Rapid detoxification of Microcystin-LR by selective catalytic hydrogenation of the Adda moiety using TiO_2-supported Pd catalysts

Jingya Sun [a,1], Kun Liu [a,1], Pedro J.J. Alvarez [b], Heyun Fu [a], Shourong Zheng [a], Daqiang Yin [c], Xiaolei Qu [a,*]

[a] State Key Laboratory of Pollution Control and Resource Reuse, School of the Environment, Nanjing University, Jiangsu, 210023, China
[b] Department of Civil and Environmental Engineering, Rice University, Houston, TX, 77005, United States
[c] State Key Laboratory of Pollution Control and Resources Reuse, College of Environmental Science and Engineering, Tongji University, Shanghai, 200092, China

HIGHLIGHTS

- Catalytic hydrogenation on Pd/TiO_2 removed MC-LR from water with fast kinetics.
- Selective catalytic hydrogenation of the Adda moiety led to effective detoxification.
- The reactions selectively targeted three C═C bonds of MC-LR in sequence.
- Surface adsorption and the cationic Pd played a key role in the reaction kinetics.

GRAPHICAL ABSTRACT

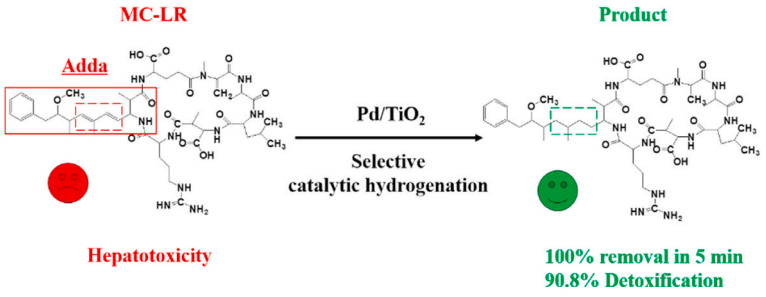

ARTICLE INFO

Handling Editor: Chang Min Park

Keywords:
Microcystin-LR
Rapid detoxification
Selective catalytic hydrogenation
Supported Pd catalysts
Metal-support interactions

ABSTRACT

The hepatotoxicity of Microcystin-LR (MC-LR) is mainly caused by its Adda moiety. In this study, we used TiO_2-supported Pd catalysts to selectively hydrogenate the C═C bonds in the Adda moiety, achieving rapid detoxification of MC-LR in water under ambient conditions. MC-LR was removed within 5 min by catalytic hydrogenation on Pd(1.0)/TiO_2 with a catalyst dosage normalized rate constant of 1.3×10^{-2} L mg_{cat}^{-1} min^{-1}, significantly more efficient than other catalytic treatment methods. The reactions proceeded in a highly selective manner towards catalytic hydrogenation at the C═C bond of the Mdha moiety and subsequently the conjugated double bond of the Adda moiety, yielding two intermediates and one final product. Upon catalytic hydrogenation for 30 min on Pd(0.07)/TiO_2, the toxicity of MC-LR (assessed by protein phosphatase 2A activity assay) drastically decreased by 90.8%, demonstrating effective detoxification. The influence of catalyst support, Pd content, initial MC-LR concentration, reaction pH, and catalytic stability were examined. Surface adsorption and the cationic Pd played a crucial role in the reaction kinetics. Our results suggest that catalytic hydrogenation is a highly effective and safe strategy for detoxifying MC-LR by selective reactions.

* Corresponding author.
E-mail address: xiaoleiqu@nju.edu.cn (X. Qu).
[1] Jingya Sun and Kun Liu contributed equally to this work.

https://doi.org/10.1016/j.chemosphere.2021.132641
Received 28 July 2021; Received in revised form 2 October 2021; Accepted 19 October 2021
Available online 20 October 2021

1. Introduction

Microcystin-LR (MC-LR) produced by cyanobacteria is one of the most widespread toxins in eutrophic waters that in many cases serve as the source of drinking water (Sharma et al., 2012; Vasconcelos et al., 1996). MC-LR can cause irreversible liver damage or cancer owing to its ability to inhibit the activity of proteins phosphatase 1 and 2A (Carmichael, 2001; Hitzfeld et al., 2000). The LD_{50} of MC-LR is 50 μg kg^{-1} bodyweight, close to the venom of Crotalus atrox (an international reference venom with an LD_{50} of 56 μg kg^{-1}) (Chorus and Welker, 2021). It was frequently found in the source water for drinking water treatment facilities around the globe and sometimes even found in the drinking water supply with concentrations as high as 3.6 μg L^{-1} (Hoeger et al., 2005; Mohamed et al., 2015). The World Health Organization has proposed a guideline of 1.0 μg L^{-1} for MC-LR in drinking water (WHO, 2017). The United States Environmental Protection Agency also included microcystins on the fourth contaminant candidate list (U.S. EPA, 2016). Therefore, the detoxification of MC-LR in water is an important treatment challenge.

MC-LR is relatively stable in water due to its cyclic and hydrophilic structure (Fig. S1). In many cases, physical treatment processes commonly used in water treatment facilities (e.g., coagulation, sedimentation, and rapid filtration) cannot sufficiently remove MC-LR due to its soluble nature (Mohamed et al., 2015; Shang et al., 2018). A variety of chemical treatment techniques to eliminate MC-LR from water have been investigated, including ozonation, chlorination, and photocatalysis (Guo et al., 2018; Kull et al., 2004; Shawwa and Smith, 2001; Zhang et al., 2019). Although these techniques can achieve effective removal of MC-LR, additional challenges remain to be addressed. Photocatalysis processes demand relatively high energy usage (Woan et al., 2009). Chlorination and ozonation processes may lead to harmful byproducts due to side reactions (Chang et al., 2014; Lu et al., 2018; von Gunten, 2003). Ozonation can lead to the formation of bromate and bromo-organic byproducts, which are harmful to human health (von Gunten, 2003). Therefore, the development of new treatment techniques capable of rapidly degrading or detoxifying MC-LR is highly desirable.

The hepatotoxicity of MC-LR is mainly caused by the covalent bonding between protein phosphatases and its Adda moiety (Carmichael and An, 1999). Reductive treatment of MC-LR provides an attractive alternative for the detoxification process since the Adda moiety of MC-LR contains double bonds. Gao et al. (2016) investigated the degradation of MC-LR by nanoscale zero-valent iron (nZVI) and found 28% of MC-LR was removed after 2 h. The activity of nZVI could be enhanced by functionalizing it with Ni or Pd, which resulted in 90% MC-LR removal in 120 min (Gao et al., 2016; Wang et al., 2014). However, nZVI-based materials are highly susceptible to deactivation even in pure waters, and are difficult to regenerate and reuse. Liquid phase catalytic hydrogenation could be a highly effective water treatment method to reductively remove undesirable chemical substances in water such as oxyanions (i.e., hydrodeoxygenation), N-nirosamines (i.e., N–N hydrogenation), and halogenated organic pollutants (i.e., hydrodehalogenation) (Huo et al., 2018; Knitt et al., 2008; Sun et al., 2018; Zheng et al., 2020). Nevertheless, catalytic strategies selectively target C═C bonds have not yet been investigated for water treatment.

Supported Pd catalysts are widely used in liquid phase catalytic hydrogenation research due to their superior capability in H_2 activation under ambient conditions (Chaplin et al., 2012). Pd can serve as a highly selective hydrogenation catalyst owing to its affinity for unsaturated bonds (Antonetti et al., 2015; Liu et al., 2020). For example, SiO_2-supported Pd catalysts exhibited high hydrogenation selectivity to C═C rather than C═O bond for cinnamaldehyde to form hydrocinnamaldehyde as the final product (Yang et al., 2012). The toxic Adda moiety of MC-LR comprised of two possible hydrogenated groups (i.e., aromatic ring and conjugated double bond), in which the conjugated double bond was mainly responsible for its hepatotoxicity (He et al., 2016).

We postulate that effective and rapid detoxification of MC-LR can be achieved by selective catalytic hydrogenation of the C═C in the Adda moiety, using supported Pd catalysts. In this work, we (1) examine the feasibility of the detoxication of MC-LR using catalytic hydrogenation on TiO_2-supported Pd catalysts; and (2) elucidate the key structural properties of supported Pd catalysts determining its catalytic activity.

2. Materials and methods

2.1. Materials

Palladium chloride (>99%) was purchased from Shanghai Chemical Reagent Co., Ltd., China. TiO_2 (P25) was purchased from Evonik Degussa, Germany. Sodium hydroxide (≥96.0%) and hydrochloric acid (≥96.0%) were purchased from Sinopharm Chemical Reagent Co., China. Sodium carbonate ((Na_2CO_3, AR) was purchased from Nanjing Chemical Reagent Co., China. Trifluoroacetic acid (TFA, ≥99.5%) was purchased from Maclin, China. MC-LR (1 mg, ≥95% purity) was purchased as lyophilized solid from Taiwan Algal Science Inc and stored in a freezer at −20 °C. Two milliliters of deionized water was added to dissolve the MC-LR standard, yielding a 500 mg L^{-1} of MC-LR stock solution. The MC-LR stock solution was stored at 4 °C in the dark and vortexed for 2 min prior to use.

2.2. Catalyst preparation

The supported Pd catalysts were prepared using the deposition-precipitation method. Briefly, 1 g of TiO_2, Al_2O_3, or SiO_2 was dispersed in 20 mL deionized water containing a desired amount of $PdCl_2$. After stirring for 2 h, Na_2CO_3 solution (1 mol L^{-1}) was added dropwise into the suspension until pH reached 10.5, and the mixture was further stirred for 2 h. The resulting solid was recovered by filtration, washed with deionized water, oven-dried at 105 °C for 6 h, and calcinated in a muffle furnace at 300 °C for 4 h. All the catalysts were pre-reduced at 300 °C for 2 h in an H_2 stream before characterization and the catalytic hydrogenation (Kang et al., 2002; Kwak et al., 2013). The synthesized catalyst was denoted as Pd(x)/TiO_2, Pd(x)/Al_2O_3, or Pd(x)/SiO_2, where x is the Pd content (wt.%) measured by the inductively coupled plasma atomic emission spectroscopy (ICP-AES, PerkinElmer Optima-5300DV, PerkinElmer, Inc., USA).

2.3. Catalyst characterization

The Pd contents of the samples were determined by the ICP-AES. The X-ray diffraction (XRD) patterns of the samples were recorded in the range of 20–80° on a Bruker D8 Advance powder diffraction-meter (BRUKER, Germany) using Cu K_α radiation (λ = 1.540562 Å). The crystalline phases were analyzed based on the standard JCPDS files. The microstructures of the catalysts were analyzed by a Tecnai G2 F20 Super Twin transmission electron microscope (TEM) at 200 eV equipped with a high angle annular dark-field (HAADF) detector (FEI, USA). The specimens were prepared by dispersing the catalysts in ethanol using an ultrasonic bath and evaporating a drop of resulting suspension onto the lacey carbon support grid. The X-ray photoelectron spectroscopy (XPS) spectra were collected on an ESCALAB 250Xi spectrometer (Thermo Scientific, USA) equipped with a monochromatized Al K_α X-ray source ($h\nu$ = 1486.6 eV) and a hemispherical analyzer. The operation condition was set to be 50 eV pass energy with a step size of 0.05 eV over an energy window of 30 eV and a pressure of 10^{-9} MPa. The C1s peak (284.6 eV) was used for the calibration of binding energy values. Nonlinear Shirley-type background subtraction was applied for all spectra. For determination of the Pd state on catalysts, the Pd 3d spectra were deconvoluted using XPSPeak41 software. The fitting lineshape of Pd^0 was derived from standard Pd powder recorded on the same conditions. The areas of fitting peaks in the Pd $3d_{5/2}$ region were used for the estimation of the $Pd^{\delta+}/Pd^0$ ratio.

The isoelectric points (IEP) of the catalysts were determined by the phase analysis light scattering (PALS) using a ZEN 3500 Zetasizer Nano ZS (Malvern, Worcestershire, U.K.). Briefly, 3 mg catalysts were dispersed in deionized water. The pH values of the suspensions were pre-adjusted at set points using HCl or NaOH solution. After equilibration for 24 h, the potentials of the suspensions were measured using the Zetasizer Nano ZS.

The particle sizes and dispersions of Pd were determined using H_2 chemisorption on a Micromeritics Autochem II chemisorption analyzer (Micromeritics Instrument Co., Norcross, GA). Two hundred milligram of catalyst was loaded in a U-shaped quartz reactor and heated to 300 °C in a 10 vol % H_2/Ar stream (30 mL min^{-1}) for 2 h to reduce the catalyst in-situ. Then, the stream was switched to an Ar stream for 1 h at 300 °C to remove the adsorbed H_2. After cooling down to room temperature, H_2 chemisorption was conducted using a pulse method. The dispersion of Pd was determined on the assumption of a unit adsorption stoichiometry from the following equation based on H_2 chemisorption data (Aramendia et al., 1996):

$$D = \frac{AU}{vW} \tag{1}$$

where A is the atomic weight of Pd (106.4 g/mol), U is the H_2 chemisorption amount using a pulse method (mol), v is the adsorption stoichiometry (0.5 mol H_2 per surface atom of Pd), and W is the amount of Pd (g).

2.4. Batch reaction

The catalytic performance of the catalysts for MC-LR hydrogenation was evaluated using a batch system in a 50 mL three-neck flask at 25 °C. The catalysts were ground to pass through a 400-mesh sieve (<37 μm) prior to the tests. Two milligrams of catalyst were dispersed in the reaction flask containing 20 mL of 2 mg L^{-1} MC-LR solution at pH 6.1. The suspension was bubbled with a N_2 flow (100 mL min^{-1}) under vigorous stirring for 15 min to remove dissolved O_2. Then the N_2 flow was switched to a H_2 flow (100 mL min^{-1}) to initiate the reaction. The high H_2 flow rate was to make sure the formation of a fully stirred reaction system in the absence of mass transfer limitations. Samples were taken at pre-determined time intervals and filtered through 0.45-μm filter membranes (ANPEL, China) for analysis. All the reactions were conducted in triplicates.

To examine the influence of reaction pH, catalytic hydrogenation reactions were conducted under environment relevant pH in the range of 6.1–9.0. The reaction pH was adjusted using a 0.1 M NaOH solution. The stability of the supported Pd catalyst for MC-LR hydrogenation was evaluated by five consecutive cycles. For each cycle, 2 mg catalyst was added to 20 mL of 2 mg L^{-1} MC-LR solution at pH 6.1. The mixture was stirred and bubbled with an N_2 flow (100 mL min^{-1}) for 15 min, and then the catalytic hydrogenation was initiated by switching the N_2 flow to an H_2 flow (100 mL min^{-1}). Samples were collected at a given time interval. After the reaction, the used catalyst was collected by filtration, washing with deionized water, oven-dried at 105 °C, and reduced in H_2 stream at 300 °C for the following reaction cycle.

Catalyst activities were evaluated by the pseudo-first-order rate constants (k_{obs}, min^{-1}), catalyst dosage normalized k_{obs} (k_0, L mg_{cat}^{-1} min^{-1}), and turnover frequencies (TOF, min^{-1}). k_{obs} was determined by fitting the natural log of MC-LR concentration versus reaction time in the initial 5 min. TOF was defined as the conversion of initial MC-LR per min normalized by surface-exposed Pd sites of the catalysts. The surface exposed Pd sites were obtained according to H_2 chemisorption data. Catalysts k_0 and TOF were determined using the following Equations (2) and (3), respectively:

$$k_0 = \frac{k_{obs}}{W_{cat}} \tag{2}$$

$$TOF = \frac{(C_0 - C_t) \times m}{W_{cat} \times M_{Pd} \times D_{cat} \times t} \tag{3}$$

where k_{obs} is pseudo-first-order rate constants (min^{-1}), W_{cat} is the catalyst dosage (mg L^{-1}), the C_0 is the initial MC-LR concentration (mmol L^{-1}), C_t is the MC-LR concentration at selected reaction time (mmol L^{-1}), m is the molar weight of Pd (106.4 g mol^{-1}), M_{Pd} is the weight percentage of Pd in catalyst, D_{cat} is the dispersion of Pd on the catalyst, and t is the selected reaction time (min). M_{Pd} and D_{cat} are dimensionless.

2.5. Analytical methods

The concentrations of MC-LR were determined using high-performance liquid chromatography (HPLC, Agilent Technologies, USA) equipped with a photo diode array detector and a 4.6 × 150 mm Zorbax Eclipse SB-C18 column (Agilent Technologies, USA). The mobile phase consisted of 65% methanol and 35% water with 0.05% TFA. The injection volume of the sample was 90 μL, and the flow rate was 0.8 mL min^{-1}. The wavelength for UV absorbance detection was 238 nm.

The analysis of the hydrogenation intermediates and products of MC-LR was performed on an HPLC (Agilent 1260 infinity) coupled to a quadrupole time-of-flight mass spectrometer (QTOF-MS, Triple TOF 5600, AB SCIEX). The intermediates and products were first chromatographically separated using a C18 column (5 μm, 150 mm × 2.1 mm, Agilent Technologies, USA) and then analyzed by scanning from m/z 100 to 2000 in positive ion mode of electrospray ionization using the mass spectrometer. The injection volume was 20 μL. The mobile phase solvents were 0.1% formic acid in water and acetonitrile with a flow rate of 0.200 mL min^{-1}. The optimized gradient elution for acetonitrile was as follows: 10% for 0–5 min, 35% for 5–10 min, 60% for 10–20 min, and 80% for 20–25 min, followed by equilibrium for 5 min with 10% acetonitrile.

The toxicity of MC-LR solutions was quantified by the PP2A activity assay using a Microcystins PP2A kit (ZEU-Immunotec, Spain) (Kim and Lee, 2019). For the assay, the linear range for MC-LR was 0.1–2 ppb. Hence, samples were diluted to yield concentrations within this range. The relative inhibition of PP2A activity was used to evaluate the toxicity of MC-LR as shown in Equation (4):

$$\%inhibition = \frac{A_c - A_t}{A_c} \times 100\% \tag{4}$$

where A_c and A_t refer to the absorbances of a PP2A control treatment and of samples containing MC-LR after t minutes of treatment, respectively.

3. Results and discussion

3.1. Catalyst characterization

We prepared a series of supported Pd catalysts with different Pd loadings and supports (i.e., TiO_2, Al_2O_3, and SiO_2, Table 1). The Pd particle size and the dispersion on different catalysts were first examined using the H_2 chemisorption method (Aramendia et al., 1996). For Pd/TiO_2, the Pd particle size increased from 1.9 nm to 2.7 nm as the Pd content increased from 0.07 wt% to 0.23 wt%, while Pd dispersion decreased from 52% to 39%. The STEM-HAADF analysis further confirmed the increase of Pd particle size with increasing Pd content. The micrographs and histograms of the Pd particle size distribution on Pd/TiO_2 are presented in Fig. S2. The average Pd particle sizes of Pd (0.16)/TiO_2 and Pd(0.23)/TiO_2 were 2.5 and 3.0 nm, respectively (Table 1, details can be found in Calculation S1). STEM-HAADF cannot accurately determine the average Pd particle size of Pd(0.07)/TiO_2 as sparse Pd particles were found in the micrographs. The reduced dispersion of Pd with increasing Pd content was attributed to the

Table 1
Structural properties of Pd particles and the catalytic performance of the supported Pd catalysts.

Catalysts	Pd content [a]	Pd size [b]	Pd size [c]	Pd dispersion [c]	$Pd^{\delta+}/Pd^0$ [d]	k_0 [e,f]	TOF [e,f]
	(wt.%)	(nm)	(nm)	(%)		(L mg_{cat}^{-1} min^{-1})	(min^{-1})
Pd (0.07)/TiO_2	0.07	–	1.9	52	1.7	3.7×10^{-3}	1.26
Pd (0.16)/TiO_2	0.16	2.5	2.2	46	0.4	7.2×10^{-3}	0.96
Pd (0.23)/TiO_2	0.23	3.0	2.7	39	0.2	6.0×10^{-3}	0.78
Pd (0.09)/Al_2O_3	0.09	–	1.8	59	0.5	2.8×10^{-4}	0.12
Pd (0.04)/SiO_2	0.04	–	1.7	62	0.2	–	–

[a] Determined by ICP-AES.
[b] Measured by TEM.
[c] Calculated based on H_2 chemisorption.
[d] Determined by XPS.
[e] The calculation of k_0 and TOF were given in the section of Materials and Methods.
[f] Reaction conditions: pH = 6.1, MC-LR concentration: 2 mg L^{-1}, catalyst dosage: 0.1 g L^{-1}.

aggregation of Pd particles on the catalysts during the calcination process (Kawawaki et al., 2021; Louis et al., 1993). XRD patterns of Pd/TiO_2 and TiO_2 support had clear diffraction peaks at 25.4°, 27.5°, 37.9°, 48.7°, 54.0°, 55.2°, and 62.8°, corresponding to the anatase and rutile phase of TiO_2 (Fig. S3). No diffraction peak of Pd or PdO was found in the spectra, likely due to the small particle sizes and low Pd contents (Li et al., 2017; Sun et al., 2017). The Pd particle sizes of Pd(0.09)/Al_2O_3, Pd (0.07)/TiO_2, and Pd(0.04)/SiO_2 were calculated to be 1.8, 1.9 and 1.7 nm, respectively, based on the H_2 chemisorption method. The dispersion of Pd was on the order of Pd(0.04)/SiO_2 > Pd(0.09)/Al_2O_3 > Pd (0.07)/TiO_2.

Pd speciation on the catalysts and Pd powder was examined by XPS measurements in the Pd 3d region (Fig. 1, Fig. S4). Since the average size of Pd particles was smaller than 3.0 nm as suggested by the TEM data, the photoelectrons of XPS were expected to penetrate the whole Pd particles (Vickerman and Gilmore, 2009). The spectra of Pd on the catalysts can be deconvoluted into two doublets assigning to the metallic Pd (Pd^0) and cationic Pd ($Pd^{\delta+}$), respectively (Table 1) (Datye et al., 2000). The binding energy of Pd^0 (335.4 eV) on the catalysts was identical to those reported values for supported Pd catalysts (Brun et al., 1999; Datye et al., 2000), which were slightly higher than that of bulk Pd powder (335.1 eV) (Fig. 1). This was caused by the photoionization phenomenon for small Pd particles on the catalysts (Takasu et al., 1978). Since all the catalysts were pre-reduced with H_2 to remove oxidized Pd before XPS analysis, the presence of $Pd^{\delta+}$ species was most likely attributed to the electron transfer from Pd to the catalyst support facilitated by the strong metal-support interactions (Herrmann et al., 1987; Tauster et al., 1981). For Pd(0.04)/SiO_2, most Pd existed in the metallic state as evident by the low $Pd^{\delta+}/Pd^0$ ratio of 0.2. A higher $Pd^{\delta+}/Pd^0$ ratio was found for Pd supported on Al_2O_3 and TiO_2. The $Pd^{\delta+}/Pd^0$ ratios of Pd(0.09)/Al_2O_3 and Pd(0.07)/TiO_2 were 0.5 and 1.7, respectively. The higher $Pd^{\delta+}/Pd^0$ ratio of Pd(0.07)/TiO_2 indicates a stronger interaction between Pd and TiO_2 than Al_2O_3 and SiO_2, consistent with the literatures (Chang et al., 1985, Tauster and Fung, 1978). The strong metal-support interaction between Pd and TiO_2 was supported by the gradual cationization of Pd (i.e., $Pd^{\delta+}/Pd^0$ increased from 0.2 to 1.7) as Pd contents decreased from 0.23 wt% to 0.07 wt%. This was because lower Pd content led to decreased average Pd particle size, which enhanced the metal-support interaction (Haller and Resasco, 1989).

3.2. Catalytic hydrogenation on Pd/TiO_2 is a highly effective approach for MC-LR removal

Catalytic hydrogenation kinetics of MC-LR on Pd/TiO_2 was examined to evaluate the performance of catalysts (Fig. 2). Pd/TiO_2 was chosen as it has the highest performance among catalysts with different supports (see detailed discussion in section 3.4). Control experiments showed that H_2 could not reduce MC-LR without catalysts. MC-LR completely disappeared within 5 min at ambient conditions in the presence of Pd(1.0)/TiO_2 under H_2 flow, indicating extremely fast catalytic elimination of MC-LR. The MC-LR removal pattern can be well-fitted by the pseudo-first-order kinetic model. The catalyst dosage normalized rate constant (k_0) was calculated to be 1.3×10^{-2} L·mg_{cat}^{-1}·min^{-1} (Fig. S5). A detailed comparison of rate constants between catalytic hydrogenation and other catalytic processes for MC-LR removal was summarized in Table S1. Catalytic hydrogenation with Pd(1.0)/TiO_2 is much faster than previously reported catalytic treatment methods. For example, the k_0 of Pd(1.0)/TiO_2 was 3–4 orders of magnitude faster than those of nZVI (1.0×10^{-6} L mg_{cat}^{-1} min^{-1}) and Fe/Pd (1.48×10^{-5} L mg_{cat}^{-1} min^{-1}) (Gao et al., 2016). Compared to the catalytic wet peroxide oxidation approach ($k_0 = 1.1 \times 10^{-4}$ L mg_{cat}^{-1} min^{-1}), catalytic hydrogenation also had a superior activity with two orders of magnitude faster k_0 (Munoz et al., 2019). These rate comparisons clearly show that the catalytic hydrogenation of MC-LR on Pd/TiO_2 is a highly effective and rapid approach for removing MC-LR in water.

For heterogeneous catalysis, the mass transfer of reactants to catalyst surfaces may limit the reaction rate when reaction kinetics is extremely fast (Singh and Vannice, 2001). To exclude the potential mass transfer limitations and further investigate the intrinsic activity of catalysts, we used catalysts with low Pd contents (0.04 wt% to 0.23 wt%) in the rest of this work. The influence of catalyst dosage on the catalytic hydrogenation kinetics of MC-LR on Pd(0.07)/TiO_2 was investigated (Fig. S6). It was found that the catalytic activity normalized by the catalyst dosage remained constant, suggesting the absence of mass transfer limitation on Pd(0.07)/TiO_2.

3.3. Hydrogenation products and reaction pathway

Solution samples were collected after the catalytic hydrogenation of MC-LR on Pd(0.07)/TiO_2 and analyzed using LC-MS to identify the reaction products. The analytical results are summarized in Fig. 3, Fig. S7,

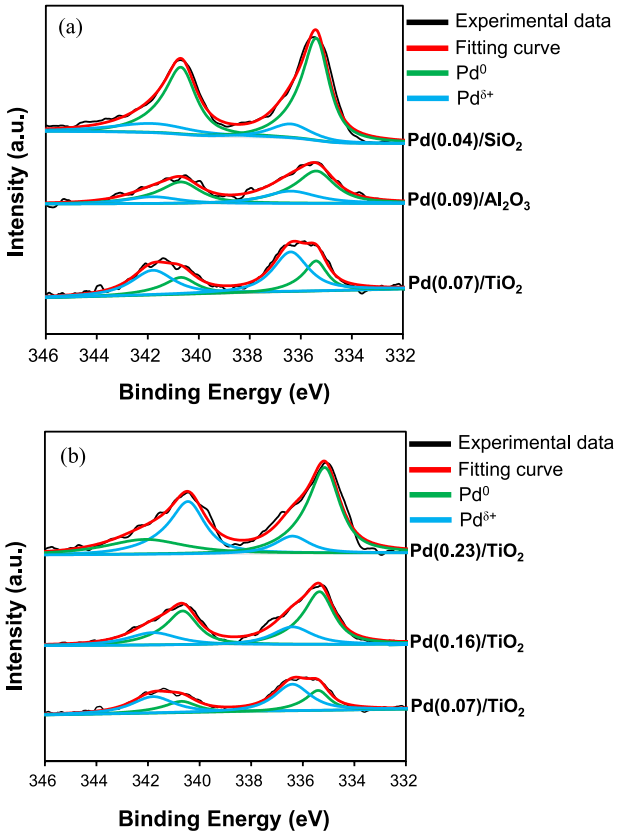

	Binding Energy of Pd $3d_{5/2}$ (eV)	
	Pd^0	$Pd^{\delta+}$
Pd powder	335.1	
$Pd(0.07)/TiO_2$	335.4	336.4
$Pd(0.16)/TiO_2$	335.4	336.4
$Pd(0.23)/TiO_2$	335.2	336.4
$Pd(0.09)/SiO_2$	335.4	336.4
$Pd(0.04)/SiO_2$	335.4	336.4

Fig. 1. XPS spectra of (a) Pd supported on different supports and (b) Pd/TiO_2 with different Pd contents in the Pd 3d region. The table summarized the binding energy of Pd in $3d_{5/2}$ region for different materials.

and Table S2. The peak at *m/z* of 995.6 was assigned to MC-LR molecules. Only three reaction products with *m/z* of 997.6, 999.6, and 1001.6 were found in the mass spectra. There were no significant peaks with *m/z* lower than 995.6 (i.e., MC-LR), indicating that the structure of MC-LR did not break down during the hydrogenation treatment. The concentrations of the reaction products could not be determined due to the lack of reference compounds. The evolution of mass spectrum peak areas of MC-LR and the reaction products was used to analyze the products and the hydrogenation pathway (Fig. 3b). The peak area of MC-LR (*m/z* 995.6) gradually decreased over time. The peak area of the product 1 (*m/z* of 997.6) exhibited a non-monotonic trend. It appeared

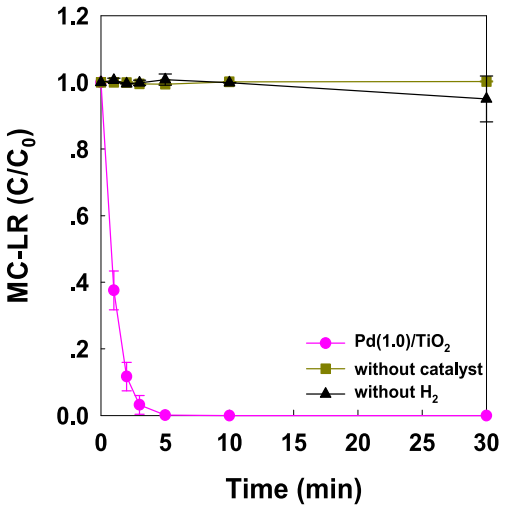

Fig. 2. Catalytic hydrogenation of MC-LR on $Pd(1.0)/TiO_2$, control experiments for MC-LR reaction under H_2 flow (100 mL min^{-1}) without catalyst and in the presence of $Pd(1.0)/TiO_2$ with H_2 flow replaced by a N_2 flow (100 mL min^{-1}). Reaction conditions: reaction pH: 6.1, catalyst dosage: 0.1 g L^{-1}, initial MC-LR concentration: 2 mg L^{-1}. Error bars represent ± one standard deviation from the mean of triplicate reaction.

immediately after the initiation of the reaction, increased at the beginning of the reaction, and decreased afterward. It was an intermediate for the overall reaction. The peak area of the product 2 (*m/z* of 999.6) appeared slightly after the generation of the product 1 and also had a volcano-like trend. It was another intermediate that was likely formed by reactions involving the product 1. The peak area of the product 3 (*m/z* of 1001.6) increased monotonically, indicating that it was the final product of the reaction. It had a brief lag time at the beginning of the reaction.

The mass differences between MC-LR and the three products were 2, 4, and 6 Da, respectively, corresponding to the addition of one, two, and three H_2 to the MC-LR molecule. We propose a sequential hydrogenation mechanism for the reactions of MC-LR on Pd-based catalysts (Fig. 3a). Pd is very active for the hydrogenation of C═C bonds due to its favorable adsorption mode for C═C bonds via planer di-σ form, whereas almost inert for the hydrogenation of aromatic ring and C═O (Delbecq and Sautet, 1995; Schwartz et al., 2016). MC-LR molecules contain three C═C bonds, including a C═C bond at the Mdha moiety and a conjugated double bond at the Adda moiety. The heat of hydrogenation of the first double bond of the conjugated system was lower than that of the C═C bond of mono-olefin, suggesting that the mono C═C bond is more easily hydrogenated than those in the conjugated system (Kistiakowsky et al., 1936). The hydrogenation pathway is proposed and shown in Fig. 3a. First, MC-LR was hydrogenated at the C═C bond of the Mdha moiety to form an intermediate with m/z of 997.6 (product 1). Then, the intermediate was successively hydrogenated at the C═C bonds of the conjugated double bond of Adda moiety to generate the second intermediate (product 2) and subsequently the final product (product 3) with m/z of 999.6 and 1001.6, respectively.

3.4. Influence of catalyst support on catalyst performance

We examined three catalyst supports (i.e., Al_2O_3, SiO_2, and TiO_2) to investigate the influence of catalyst supports on the catalyst performance (Fig. 4). For $Pd(0.04)/SiO_2$, little MC-LR was removed in 30 min. $Pd(0.09)/Al_2O_3$ exhibited significant catalytic activity for MC-LR hydrogenation with 56% MC-LR removed in 30 min. $Pd(0.07)/TiO_2$ had the best performance with the complete removal of MC-LR within 30 min. Considering that these catalysts had similar Pd particle sizes (Table 1), their differed activities were related to the surface adsorption

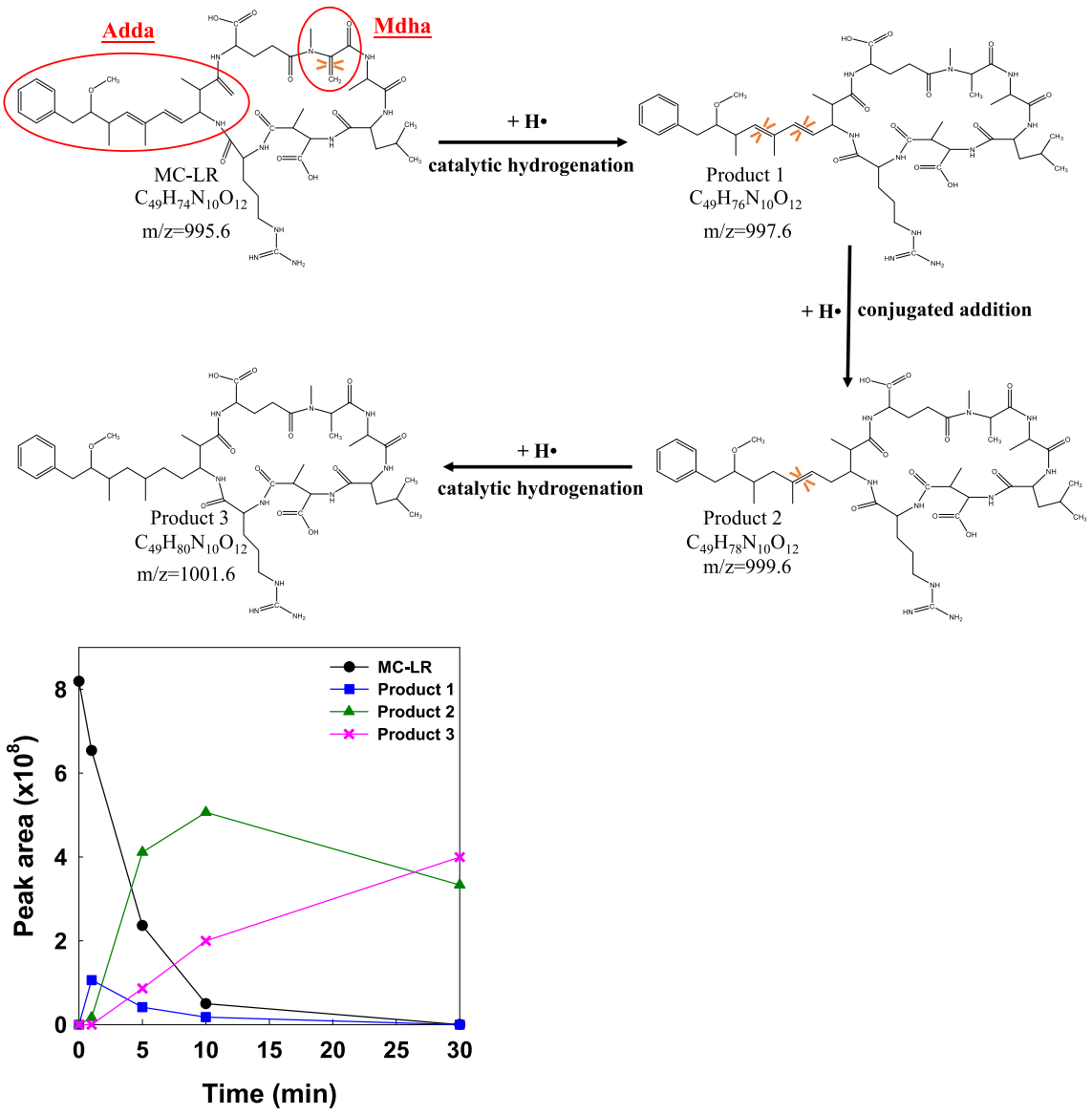

Fig. 3. (a) Catalytic hydrogenation pathways of MC-LR. (b) The evolution of LC-MS peak areas of MC-LR and the products with reaction time. Reaction conditions: catalyst: Pd(0.07)/TiO_2, reaction pH: 6.1, catalyst dosage: 0.1 g L^{-1}, initial MC-LR concentration: 2 mg L^{-1}.

and the speciation of Pd. The adsorption of reactant to catalyst surface is a prerequisite process for the reaction, which is mainly controlled by the properties of the support. At a reaction pH of 6.1, MC-LR molecules (p*K*a 3.3) were negatively charged (Walker, 2014). The surface of SiO_2 was negatively charged at pH 6.1 (IEP of 1.34, ζ-potential measurements can be found in Fig. S8). Significant electrostatic repulsive interactions occurred between SiO_2 surface and MC-LR molecules at reaction conditions, leading to negligible MC-LR conversion on Pd/SiO_2. The IEP of TiO_2 and Al_2O_3 were ~6.5 and 8.0, respectively. They were positively charged at reaction pH, favoring the adsorption of MC-LR molecules. A similar support-dependent phenomenon was reported for the catalytic hydrogenation of bromate and chloroacetic acids (Chen et al., 2010; Zhou et al., 2013).

The significance of MC-LR adsorption on its hydrogenation was further examined by the influence of initial MC-LR concentrations (Fig. S9). Results showed that the reaction k_0 increased from 2.2×10^{-3} L mg_{cat}^{-1} min^{-1} to 6.4×10^{-3} L mg_{cat}^{-1} min^{-1} as the initial MC-LR concentration increasing from 0.83 mg L^{-1} to 3.78 mg L^{-1}. The data were fitted with the Langmuir-Hinshelwood model. A good linear correlation ($R^2 = 0.999$) between $1/r_0$ and $1/c_0$ was obtained (Calculation S2). This suggests that catalytic hydrogenation of MC-LR is controlled by the surface adsorption of MC-LR on the catalysts. The important role of adsorption also explained the change of catalytic activity with reaction pH (Fig. S10). Increasing the reaction pH from 6.1 to 9.0 resulted in a decrease of k_0 from 3.7×10^{-3} L mg_{cat}^{-1} min^{-1} to 1.3×10^{-3} L mg_{cat}^{-1} min^{-1}. This was caused by the reduced adsorption of MC-LR on the TiO_2 surface at high reaction pH. In addition to the surface adsorption, the differed Pd speciation on TiO_2, Al_2O_3, and SiO_2 supports also contributed to the different catalyst performance as discussed in the following section.

3.5. Cationic Pd plays a key role in the hydrogenation of MC-LR

The properties of active metal Pd are important factors in determining hydrogenation activity. The catalytic hydrogenation of MC-LR on Pd/TiO_2 with different Pd contents (Fig. S11). Catalyst TOF values were calculated and compared to investigate the intrinsic relationship between Pd sites and catalytic activity (Table 1). The TOF values followed an order of Pd(0.07)/TiO_2 (1.26 min^{-1}) > Pd(0.16)/TiO_2 (0.96 min^{-1}) > Pd(0.23)/TiO_2 (0.78 min^{-1}), indicating a decreased catalytic

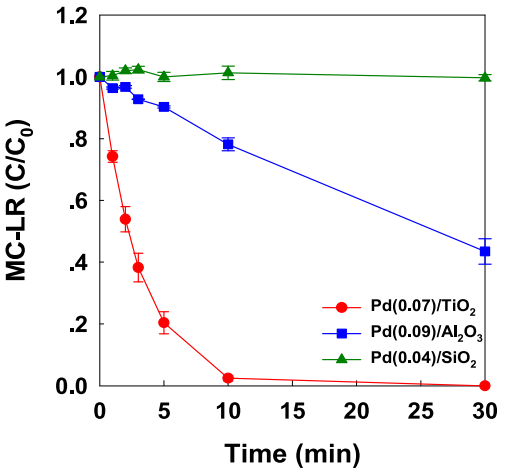

Fig. 4. Catalytic hydrogenation of MC-LR on Pd supported catalysts. Reaction conditions: reaction pH: 6.1, catalyst dosage: 0.1 g L^{-1}, initial MC-LR concentration: 2 mg L^{-1}. Error bars represent ± one standard deviation from the mean of triplicate reaction.

activity of exposed Pd site with increasing Pd content. Based on the H_2 chemisorption and XPS results, Pd/TiO_2 with higher Pd content has larger and more metallic state Pd particles. In principle, large Pd particles benefit H_2 dissociation because of enhanced H_2 spillover and high active β-PdH species (Amorim and Keane, 2008; Aramendia et al., 1999). Cationic Pd sites have higher adsorption affinity to C═C bond and favorable adsorption interaction with MC-LR (Huang et al., 1998). The decreased TOF with increasing Pd contents suggested that MC-LR adsorption and activation of C═C bonds on cationic Pd sites play more important roles in the catalytic hydrogenation of MC-LR than the H_2 activation. The vital role of cationic Pd sites also explains the higher catalytic activity of Pd(0.07)/TiO_2 than that of Pd(0.09)/Al_2O_3 and Pd (0.04)/SiO_2, as a higher content of cationic Pd sites found on Pd (0.07)/TiO_2.

3.6. Rapid detoxification of MC-LR

The changes in the toxicity of MC-LR solution during the catalytic hydrogenation on Pd(0.07)/TiO_2 are presented in Fig. 5a. The relative inhibition rate of PP2A activity of MC-LR solution remarkably decreased from 100% to 9.2% after 30 min reaction. The decrease of the toxicity generally exhibited a positive linear correlation to the decrease of the MC-LR concentration (Fig. 5b). This demonstrates that effective detoxification of MC-LR can be achieved through the catalytic hydrogenation process. There was still a 9.2% relative inhibition rate of PP2A activity left after the complete reduction of MC-LR. It suggests that specific structures of MC-LR other than the three C═C bonds targeted by Pd/TiO_2 can also induce toxic effects. Nevertheless, the residual relative inhibition rate of PP2A activity after the catalytic hydrogenation was much lower than the 23% relative inhibition rate using the solar/chlorine treatment method (Zhang et al., 2019).

3.7. Catalyst stability

Consecutive catalytic cycles were conducted to test the reusability of Pd/TiO_2 (Fig. S12). After five cycles, the reaction k_0 of Pd(0.07)/TiO_2 decreased from 3.7×10^{-3} to 1.3×10^{-3} L mg_{cat}^{-1} min^{-1}. Leaching of active sites in the reaction was considered one of the main reasons for the loss of catalytic activity (Li et al., 2019a, 2019b). The ICP measurement showed that about 33% of Pd on the catalyst was lost after 5 catalytic cycles.

4. Conclusions

This study highlights the potential of catalytic hydrogenation using supported Pd catalysts as a highly effective strategy for the rapid removal and effective detoxification of MC-LR in water at ambient conditions. The reaction proceeded in a highly selective manner towards catalytic hydrogenation at the C═C bond of the Mdha moiety and subsequently the conjugated double bond of the Adda moiety. The rest of the MC-LR structure was left intact, resulting in simple and clear reaction pathways. This is drastically different from advanced oxidation approaches that often generate a wide range of reaction byproducts, resulting in significant residual toxicity. Previously, liquid phase catalytic hydrogenation was mainly used to selectively break C-halogen, N–N, N–O, and halogen-O bonds. Our results suggest that catalytic hydrogenation targeting the C═C bonds is a promising strategy for the rapid detoxification of MC-LR and other pollutants with toxicity related to these moieties. Nevertheless, further research and development need to be conducted to improve the catalyst stability.

Credit author statement

Jingya Sun and Kun Liu: Investigation, Methodology, Writing-original draft. Pedro J.J. Alvarez: Methodology, Writing-review &

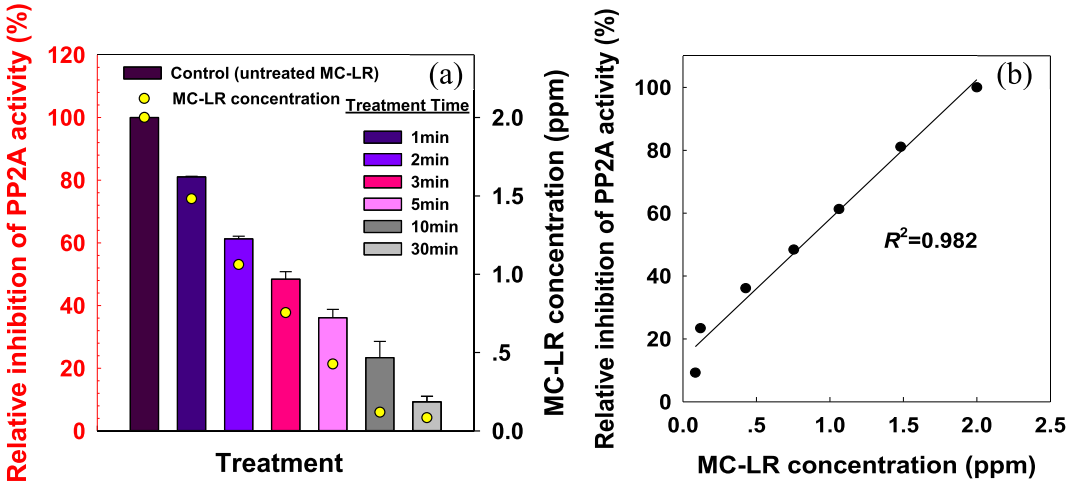

Fig. 5. (a) Evolution of the toxicity of MC-LR solution treated by catalytic hydrogenation on Pd(0.07)/TiO_2. (b) The correlation between MC-LR concentration and its toxicity. Reaction conditions: reaction pH: 6.1, catalyst dosage: 0.1 g L^{-1}, initial MC-LR concentration: 2 mg L^{-1}. Error bars represent ± one standard deviation from the mean of triplicate measurements.

editing. Heyun Fu: Methodology, Writing-review & editing. Shourong Zheng: Supervision, Writing-review & editing. Daqiang Yin: Writing-review & editing. Xiaolei Qu: Conceptualization, Supervision, Writing-review & editing. All author discussed the results and commented on the articles.

Declaration of competing interest

The authors declare that they have no known competing financial interests or personal relationships that could have appeared to influence the work reported in this paper.

Acknowledgements

This work was supported by the National Natural Science Foundation of China (Grant 21876075), the National Key Research and Development Program of China (2019YFC1804201 and 2020YFC1807002), and the NSF ERC, U.S.A on Nanotechnology-Enabled Water Treatment (EEC-1449500).

Appendix A. Supplementary data

Supplementary data to this article can be found online at https://doi.org/10.1016/j.chemosphere.2021.132641.

References

Amorim, C., Keane, M.A., 2008. Palladium supported on structured and nonstructured carbon: a consideration of Pd particle size and the nature of reactive hydrogen. J. Colloid Interface Sci. 322 (1), 196–208.

Antonetti, C., Toniolo, L., Cavinato, G., Forte, C., Ghignoli, C., Ishak, R., Cavani, F., Galletti, A.M.R., 2015. A hybrid polyketone-SiO_2 support for palladium catalysts and their applications in cinnamaldehyde hydrogenation and in 1-phenylethanol oxidation. Appl. Catal. Gen. 496, 40–50.

Aramendia, M.A., Borau, V., Garcia, I.M., Jimenez, C., Lafont, F., Marinas, A., Marinas, J. M., Urbano, F.J., 1999. Influence of the reaction conditions and catalytic properties on the liquid-phase hydrodechlorination of chlorobenzene over palladium-supported catalysts: activity and deactivation. J. Catal. 187 (2), 392–399.

Aramendia, M.A., Borau, V., Jimenez, C., Marinas, J.M., Moreno, A., 1996. Comparative measurements of the dispersion of Pd catalyst on SiO_2-$AlPO_4$ support using TEM and H_2 chemisorption. Colloids Surf., A 106, 161–165.

Brun, M., Berthet, A., Bertolini, J.C., 1999. XPS, AES and Auger parameter of Pd and PdO. J. Electron Spectrosc. 104 (1–3), 55–60.

Carmichael, W.W., 2001. Health effects of toxin-producing cyanobacteria: "The CyanoHABs". Hum. Ecol. Risk Assess. 7 (5), 1393–1407.

Carmichael, W.W., An, J.S., 1999. Using an enzyme linked immunosorbent assay (ELISA) and a protein phosphatase inhibition assay (PPIA) for the detection of microcystins and nodularins. Nat. Toxins 7 (6), 377–385.

Chang, J., Chen, Z.L., Wang, Z., Shen, J.M., Chen, Q., Kang, J., Yang, L., Liu, X.W., Nie, C. X., 2014. Ozonation degradation of microcystin-LR in aqueous solution: intermediates, byproducts and pathways. Water Res. 63, 52–61.

Chang, T.C., Chen, J.J., Yeh, C.T., 1985. Temperature-programmed reduction and temperature-resolved sorption studies of strong metal support interaction in supported palladium catalysts. J. Catal. 96 (1), 51–57.

Chaplin, B.P., Reinhard, M., Schneider, W.F., Schuth, C., Shapley, J.R., Strathmann, T.J., Werth, C.J., 2012. Critical review of Pd-based catalytic treatment of priority contaminants in water. Environ. Sci. Technol. 46 (7), 3655–3670.

Chen, H., Xu, Z.Y., Wan, H.Q., Zheng, J.Z., Yin, D.Q., Zheng, S.R., 2010. Aqueous bromate reduction by catalytic hydrogenation over Pd/Al_2O_3 catalysts. Appl. Catal. B Environ. 96 (3–4), 307–313.

Chorus, I., Welker, M., 2021. Toxic Cyanobacteria in Water: A Guide to Their Public Health Consequences. CRC Press, Boca Raton (FL), second ed. on behalf of the World Health Organization, Geneva, CH.

Datye, A.K., Bravo, J., Nelson, T.R., Atanasova, P., Lyubovsky, M., Pfefferle, L., 2000. Catalyst microstructure and methane oxidation reactivity during the Pd <-> PdO transformation on alumina supports. Appl. Catal. Gen. 198 (1–2), 179–196.

Delbecq, F., Sautet, P., 1995. Competitive C=C and C=O adsorption of alpha-beta-unsaturated aldehydes on Pt and Pd surfaces in relation with the selectivity of hydrogenation reactions——a theoretical approach. J. Catal. 152 (2), 217–236.

Gao, Y., Wang, F.F., Wu, Y., Naidu, R., Chen, Z.L., 2016. Comparison of degradation mechanisms of microcystin-LR using nanoscale zero-valent iron (nZVI) and bimetallic Fe/Ni and Fe/Pd nanoparticles. Chem. Eng. J. 285, 459–466.

Guo, Q., Li, H., Zhang, Q., Zhang, Y.L., 2018. Fabrication, characterization and mechanism of a novel Z-scheme Ag_3PO_4/NG/polyimide composite photocatalyst for microcystin-LR degradation. Appl. Catal. B Environ. 229, 192–203.

Haller, G.L., Resasco, D.E., 1989. Metal support interaction - group-viii metals and reducible oxides. Adv. Catal. 36, 173–235.

He, X.X., Liu, Y.L., Conklin, A., Westrick, J., Weavers, L.K., Dionysiou, D.D., Lenhart, J.J., Mouser, P.J., Szlag, D., Walker, H.W., 2016. Toxic cyanobacteria and drinking water: impacts, detection, and treatment. Harmful Algae 54, 174–193.

Herrmann, J.M., Gravellerumeaumaillot, M., Gravelle, P.C., 1987. A microcalorimetric study of metal support interaction in the Pt/TiO_2 system. J. Catal. 104 (1), 136–146.

Hitzfeld, B.C., Hoger, S.J., Dietrich, D.R., 2000. Cyanobacterial toxins: removal during drinking water treatment, and human risk assessment. Environ. Health Perspect. 108, 113–122.

Hoeger, S.J., Hitzfeld, B.C., Dietrich, D.R., 2005. Occurrence and elimination of cyanobacterial toxins in drinking water treatment plants. Toxicol. Appl. Pharmacol. 203 (3), 231–242.

Huang, D.C., Chang, K.H., Pong, W.F., Tseng, P.K., Hung, K.J., Huang, W.F., 1998. Effect of Ag-promotion on Pd catalysts by XANES. Catal. Lett. 53 (3–4), 155–159.

Huo, X.C., Liu, J.Y., Strathmann, T.J., 2018. Ruthenium catalysts for the reduction of N-Nitrosamine water contaminants. Environ. Sci. Technol. 52 (7), 4235–4243.

Kang, J.H., Shin, E.W., Kim, W.J., Park, J.D., Moon, S.H., 2002. Selective hydrogenation of acetylene on TiO_2-added Pd catalysts. J. Catal. 208 (2), 310–320.

Kawawaki, T., Kataoka, Y., Hirata, M., Akinaga, Y., Takahata, R., Wakamatsu, K., Fujiki, Y., Kataoka, M., Kikkawa, S., Alotabi, A.S., Hossain, S., Osborn, D.J., Teranishi, T., Andersson, G.G., Metha, G.F., Yamazoe, S., Negishi, Y., 2021. Creation of high-performance heterogeneous photocatalysts by controlling ligand desorption and particle size of gold Nanocluster. Angew. Chem. Int. Ed. 133, 21510–21520.

Kim, M.S., Lee, C., 2019. Ozonation of microcystins: kinetics and toxicity decrease. Environ. Sci. Technol. 53 (11), 6427–6435.

Kistiakowsky, G.B., Ruhoff, J.R., Smith, H.A., Vaughan, W.E., 1936. Heats of organic reactions. IV. Hydrogenation of some dienes and of benzene. J. Am. Chem. Soc. 58, 146–153.

Knitt, L.E., Shapley, J.R., Strathmann, T.J., 2008. Rapid metal-catalyzed hydrodehalogenation of iodinated X-ray contrast media. Environ. Sci. Technol. 42 (2), 577–583.

Kull, T.P.J., Backlund, P.H., Karlsson, K.M., Meriluoto, J.A.O., 2004. Oxidation of the cyanobacterial hepatotoxin microcystin-LR by chlorine dioxide: reaction kinetics, characterization, and toxicity of reaction products. Environ. Sci. Technol. 38 (22), 6025–6031.

Kwak, J.H., Kovarik, L., Szanyi, J., 2013. Heterogeneous catalysis on atomically dispersed supported metals: CO_2 reduction on multifunctional Pd catalysts. ACS Catal. 3 (9), 2094–2100.

Li, M.H., He, J., Tang, Y.Q., Sun, J.Y., Fu, H.Y., Wan, Y.Q., Qu, X.L., Xu, Z.Y., Zheng, S.R., 2019a. Liquid phase catalytic hydrogenation reduction of Cr(VI) using highly stable and active Pd/CNT catalysts coated by N-doped carbon. Chemosphere 217, 742–753.

Li, M.H., Hu, Y., Fu, H.Y., Qu, X.L., Xu, Z.Y., Zheng, S.R., 2019b. Pt embedded in carbon rods of N-doped CMK-3 as a highly active and stable catalyst for catalytic hydrogenation reduction of bromate. Chem. Commun. 55 (78), 11786–11789.

Li, Y.B., Zhang, C.B., Ma, J.Z., Chen, M., Deng, H., He, H., 2017. High temperature reduction dramatically promotes Pd/TiO_2 catalyst for ambient formaldehyde oxidation. Appl. Catal. B Environ. 217, 560–569.

Liu, Y.N., Fu, F.Z., McCue, A., Jones, W., Rao, D.M., Feng, J.T., He, Y.F., Li, D.Q., 2020. Adsorbate-induced structural evolution of Pd catalyst for selective hydrogenation of acetylene. ACS Catal. 10 (24), 15048–15059.

Louis, C., Cheng, Z.X., Che, M., 1993. Characterization of Ni/SiO_2 catalysts during impregnation and further thermal-activation treatment leading to metal particles. J. Phys. Chem. 97 (21), 5703–5712.

Lu, S.Y., Wang, N.Y., Wang, C., 2018. Oxidation and biotoxicity assessment of microcystin-LR using different AOPs based on UV, O_3 and H_2O_2. Front. Environ. Sci. Eng. 12 (3).

Mohamed, Z.A., Deyab, M.A., Abou-Dobara, M.I., El-Sayed, A.K., El-Raghi, W.M., 2015. Occurrence of cyanobacteria and microcystin toxins in raw and treated waters of the Nile River, Egypt: implication for water treatment and human health. Environ. Sci. Pollut. Res. 22 (15), 11716–11727.

Munoz, M., Nieto-Sandoval, J., Cires, S., de Pedro, Z.M., Quesada, A., Casas, J.A., 2019. Degradation of widespread cyanotoxins with high impact in drinking water (microcystins, cylindrospermopsin, anatoxin-a and saxitoxin) by CWPO. Water Res. 163, 114853.

Schwartz, T.J., Lyman, S.D., Motagamwala, A.H., Mellmer, M.A., Dumesic, J.A., 2016. Selective hydrogenation of unsaturated carbon-carbon bonds in aromatic-containing platform molecules. ACS Catal. 6 (3), 2047–2054.

Shang, L.X., Feng, M.H., Xu, X.E., Liu, F.F., Ke, F., Li, W.C., 2018. Co-occurrence of microcystins and taste-and-odor compounds in drinking water source and their removal in a full-scale drinking water treatment plant. Toxins 10, 26.

Sharma, V.K., Triantis, T.M., Antoniou, M.G., He, X.X., Pelaez, M., Han, C.S., Song, W.H., O'Shea, K.E., de la Cruz, A.A., Kaloudis, T., Hiskia, A., Dionysiou, D.D., 2012. Destruction of microcystins by conventional and advanced oxidation processes: a review. Separ. Purif. Technol. 91, 3–17.

Shawwa, A.R., Smith, D.W., 2001. Kinetics of microcystin-LR oxidation by ozone. Ozone: Sci. Eng. 23 (2), 161–170.

Singh, U.K., Vannice, M.A., 2001. Kinetics of liquid-phase hydrogenation reactions over supported metal catalysts-a review. Appl. Catal. Gen. 213 (1), 1–24.

Sun, J.Y., Han, Y.X., Fu, H.Y., Qu, X.L., Xu, Z.Y., Zheng, S.R., 2017. Au@Pd/TiO_2 with atomically dispersed Pd as highly active catalyst for solvent-free aerobic oxidation of benzyl alcohol. Chem. Eng. J. 313, 1–9.

Sun, J.Y., Zhang, J.R., Fu, H.Y., Wan, H.Q., Wan, Y.Q., Qu, X.L., Xu, Z.Y., Yin, D.Q., Zheng, S.R., 2018. Enhanced catalytic hydrogenation reduction of bromate on Pd catalyst supported on CeO_2 modified SBA-15 prepared by strong electrostatic adsorption. Appl. Catal. B Environ. 229, 32–40.

Takasu, Y., Unwin, R., Tesche, B., Bradshaw, A.M., Grunze, M., 1978. Photoemission from palladium particle arrays on an amorphous silica substrate. Surf. Sci. 77 (2), 219–232.

Tauster, S.J., Fung, S.C., 1978. Strong metal-support interactions: occurrence among the binary oxides of groups IIA-VB. J. Catal. 55 (1), 29–35.

Tauster, S.J., Fung, S.C., Baker, R.T.K., Horsley, J.A., 1981. Strong-interactions in supported-metal catalysts. Science 211 (4487), 1121–1125.

U.S. Environmental Protection Agency, 2016. Contaminant Candidate List (CCL) and Regulatory Determination. U.S. Environmental Protection Agency, Washington, DC. https://www.epa.gov/ccl/chemical-contaminants-ccl-4. (Accessed 16 June 2021). Accessed.

Vasconcelos, V.M., Sivonen, K., Evans, W.R., Carmichael, W.W., Namikoshi, M., 1996. Hepatotoxic microcystin diversity in cyanobacterial blooms collected in Portuguese freshwaters. Water Res. 30 (10), 2377–2384.

Vickerman, J.C., Gilmore, I.S., 2009. Surface Analysis –The Principal Techniques, second ed. JohnWiley & Sons Ltd, The Atrium, Southern Gate, Chichester,West Sussex, PO19 8SQ, United Kingdom.

von Gunten, U., 2003. Ozonation of drinking water: part II. Disinfection and by-product formation in presence of bromide, iodide or chlorine. Water Res. 37 (7), 1469–1487.

Walker, H.W., 2014. Harmful Algae Blooms in Drinking Water: Removal of Cyanobacterial Cells and Toxins. CRC Press, Boca Raton, U.S.

Wang, F.F., Gao, Y., Sun, Q., Chen, Z.L., Megharaj, M., Naidu, R., 2014. Degradation of microcystin-LR using functional clay supported bimetallic Fe/Pd nanoparticles based on adsorption and reduction. Chem. Eng. J. 255, 55–62.

World Health Organization (WHO), 2017. Guidelines for Drinking-Water Quality, fourth ed. World Health Organization, Geneva, Switzerland https://www.who.int/publications/i/item/9789241549950. (Accessed 16 June 2021). Accessed.

Woan, K., Pyrgiotakis, G., Sigmund, W., 2009. Photocatalytic carbon-nanotube-TiO_2 composites. Adv. Mater. 21 (21), 2233–2239.

Yang, X., Chen, D., Liao, S.J., Song, H.Y., Li, Y.W., Fu, Z.Y., Su, Y.L., 2012. High-performance Pd-Au bimetallic catalyst with mesoporous silica nanoparticles as support and its catalysis of cinnamaldehyde hydrogenation. J. Catal. 291, 36–43.

Zhang, X.R., He, J., Lei, Y., Qiu, Z.M., Cheng, S.S., Yang, X., 2019. Combining solar irradiation with chlorination enhances the photochemical decomposition of microcystin-LR. Water Res. 159, 324–332.

Zheng, C.L., Li, M.H., Liu, H., Xu, Z.Y., 2020. Complete dehalogenation of bromochloroacetic acid by liquid phase catalytic hydrogenation over Pd/CeO_2 catalysts. Chemosphere 239, 124740.

Zhou, J., Han, Y.X., Wang, W.J., Xu, Z.Y., Wan, H.Q., Yin, D.Q., Zheng, S.R., Zhu, D.Q., 2013. Reductive removal of chloroacetic acids by catalytic hydrodechlorination over Pd/ZrO_2 catalysts. Appl. Catal. B Environ. 134, 222–230.